Ensemble-based snow depth data assimilation for a multi-layer snow scheme over the European Arctic

Åsmund Bakketun[1,2], Jostein Blyverket[1], and Malte Müller[1,2]

[1]Development Centre for Weather Forecasting, Norwegian Meteorological Institute, Oslo, Norway
[2]Department of Geosciences, University of Oslo, Oslo, Norway

Correspondence: Åsmund Bakketun (asmundb@met.no)

Abstract. Reliable estimates of Earth system conditions are important for weather forecasting, hydrological modelling and their downstream applications. Both real-time prediction systems and historical reanalyses use a combination of observations and physical laws embedded in numerical models to generate gapless and accurate estimates of weather, climate and hydrological conditions. Data assimilation systems merge information from the two sources in an objective way, accounting for their respective uncertainties. In this work we present a regional reanalysis system, focusing on the land surface component. The system uses a multi-layer snow model together with the ensemble-based Local Ensemble Transform Kalman Filter (LETKF) data assimilation scheme. The system is run for a 4 year period over the European Arctic, assimilating in situ snow depth observations. Evaluation of the snow depth estimates showed reduced errors compared to existing products and positive impact of the data assimilation over the domain. Furthermore, a significant difference in total accumulated snow water was seen over the domain, implying a potential impact on downstream hydrological applications. The ensemble correlations between the total snow depth and the relatively large control vector indicated that the ensemble was able to represent snow compaction processes. The LETKF is thus able to account for these processes, which are often neglected in snow depth data assimilation. The system presented in this study allows for future extensions, including other types of observations and analyses beyond snow variables.

1 Introduction

Accurate weather and climate estimates are crucial for a wide range of applications, including advancing our knowledge of the Earth system. In mountain regions and high latitudes, seasonal snow cover significantly influences land-atmosphere interactions. This is due to its high albedo, which reflects more sunlight compared to snow-free ground and its unique thermal properties (Gong et al., 2004). Moreover, realistic initial conditions of surface and snow variables play a key role in improving atmospheric predictions (de Rosnay et al., 2014). Seasonal snow cover also impacts local infrastructure and stores substantial amounts of water, which are released during spring melt (Viviroli et al., 2007; Sturm et al., 2017; Croce et al., 2018). Accurate estimates of snow cover and mass are also vital for managing hydropower stations and issuing timely flood warnings (Casson et al., 2018; Li et al., 2019; Magnusson et al., 2020).

Reanalysis products offer consistent time series of meteorological conditions on both global (Hersbach et al., 2020) and
regional scales (Schyberg H. et al., 2021). By integrating vast amounts of observational data into numerical model simulations,
they generate estimates of numerous parameters. Among these, global atmospheric reanalyses like ERA5 (Hersbach et al.,
2020) and MERRA-2 Gelaro et al. (2017) have become foundational tools in Earth system research.

The land surface component of numerical weather prediction models, is often simplified compared to state of the art models
used in other communities (Fisher and Koven, 2020). Land surface models can be run stand-alone using atmospheric input
from a forecast or reanalysis product. This allows for efficient testing of new configurations and production of datasets tailored
for specific needs (Arduini et al., 2019; Zsoter et al., 2022). Several reanalyses feature a stand-alone "spin off" prioritizing
improved representation of land surface processes. One such example is ERA5-Land, derived from ERA5. It incorporates a
more advanced surface model and has a higher spatial resolution compared to the ERA5 dataset (Muñoz-Sabater et al., 2021).
Despite the improved representation of the land surface, several challenges remain to be solved. Cao et al. (2020) found warm
bias in ERA5-Land soil temperature in high latitudes affecting permafrost estimation, potentially due to snow density errors.
Clelland et al. (2024) found no advantage of ERA5-Land relative to ERA5 over Siberia for a range of climate variables. Kouki
et al. (2023) used satellite retrievals of snow variables to demonstrate improved spatial snow cover estimates in ERA5-land,
but overestimated snow water equivalent particularly in high elevation areas compared to ERA5.

Regional reanalyses add value to the global reanalyses by providing higher resolution products over limited geographical
areas (Køltzow et al., 2022). Notable examples include the Copernicus European and Arctic regional reanalysis products
CERRA (Ridal et al., 2024) and CARRA (Schyberg H. et al., 2021), among others. They use the ERA5 global product as
lateral boundary conditions and optimize observation usage and parametrization over Europe and the European Arctic region.
Nevertheless, these products are based on simple land surface schemes which are not able to describe important processes.
Monteiro et al. (2024) configured a multi-layer land surface model and improved the representation of seasonal snow in a
numerical weather prediction system similar to the one used in the production of CARRA. While a reported evaluation of snow
properties is missing for the CARRA dataset, it is likely to share similar deficiencies as the single layer snow scheme in the
last mentioned study.

An essential component of reanalysis systems is data assimilation. Data assimilation is the method of combining model
predictions and observations objectively based on their respective uncertainties. For snow analysis, observations often include
in situ networks of snow depth measurements, satellite observations of reflectance and microwave radiance (De Lannoy et al.,
2012; de Rosnay et al., 2014; Charrois et al., 2016; Micheletty et al., 2022; Gichamo and Draper, 2022). Furthermore, land
surface temperature products have been found useful in improving snow estimates (Alonso-González et al., 2023). Sentinel-1
backscatter data have also shown promising results for both snow depth estimates and downstream river discharge (Brangers
et al., 2024). Data assimilation schemes vary from direct insertion, which disregards the respective uncertainties (Hedrick et al.,
2018), optimal interpolation techniques using static prescribed uncertainties (Brasnett, 1999) and ensemble-based schemes
where the uncertainties are deducted from the ensemble covariances. Variants of the Ensemble Kalman Filter (EnKF) (Evensen,
2003; Tippett et al., 2003) and the particle filter (Magnusson et al., 2017; Cluzet et al., 2021; Alonso-González et al., 2023) are
popular in snow data assimilation. While the EnKF have an underlying assumption of normally distributed errors, the particle

filter is relaxed on this constraint. However, the Ensemble Kalman Filter has shown to be robust also when the Gaussian
60   assumption is not met (Katzfuss et al., 2016).

In this work, we implement a regional land reanalysis system using recent developments of the multi-layer snow model
together with an ensemble-based data assimilation scheme. Through evaluation over northern Scandinavia, we assess whether
a more advanced system can enhance estimates of snow conditions compared to those using simplified schemes. Understanding
the differences between simplified and more advanced schemes is valuable for the development of future reanalysis and weather
65   prediction systems.

The configuration of the system and reference datasets are described in Sect. 2. Results and evaluation are presented in
Sect. 3 and discussed in Sect. 4. Conclusion is given in Sect. 5.

2   Methods and data

In the following section, a brief description of the reference system (CARRA) is given, including details about its snow data
70   assimilation scheme (2.1). Subsequently, the section presents the land surface model (Sect. 2.2), data assimilation method
(Sect. 2.3), the ensemble generation and conditioning methods (Sect. 2.4-Sect. 2.5), the experimental setup in Sect. 2.7 and
finally a description of the observation and validation data (Sect. 2.6).

2.1   Copernicus Arctic Regional Reanalysis

The CARRA dataset is produced by the convection-permitting numerical weather prediction model system HARMONIE-
75   AROME (HIRLAM–ALADIN Research on Mesoscale Operational NWP in Euromed–Application of Research to Operations
at MEsoscale) (Bengtsson et al., 2017). As we focus on the snow component of the reanalysis, we guide the reader to the full
system documentation (Schyberg H. et al., 2021) for details concerning the remaining components.

The CARRA system uses the externalized surface (SURFEX) (Masson et al., 2013) as lower boundary in the model inte-
gration. The soil and snow is modelled by the force restore version of Interactions between Soil, Biosphere and Atmosphere
80   (ISBA) (Noilhan and Mahfouf, 1996; Calvet et al., 1998; Decharme et al., 2011), where two soil layers represent rapid (hourly)
and slow (daily) variations in temperature to provide fluxes back to the atmospheric component Noilhan and Mahfouf (1996).
The snow is represented by a single layer scheme (Douville et al., 1995). This snow model represents the snowpack with snow
water equivalent, snow density and albedo as prognostic variables.

In the CARRA system, in situ snow depth measurements and a binary satellite snow cover product are assimilated to update
85   snow water equivalent of the model. The in situ snow depth observations are converted to snow water equivalent using monthly
climatological snow densities from a lookup table. The satellite snow extent data is converted to snow water equivalent pseudo
observations following a set of rules. If the satellite reports "no snow", the pseudo observation yields $0 \ \mathrm{kgm^{-2}}$; if the satellite
reports "snow", the pseudo observation is set equal to the model background value in the observation point. However, if the
model exceeds $25 \ \mathrm{kgm^{-3}}$, "snow" observations are discarded, and if the model exceeds $100 \ \mathrm{kgm^{-2}}$, "no snow" observations
90   are discarded. The pseudo observation snow water equivalent value is then treated as an in situ observation. The satellite product

and assimilation method are reported in Homleid and Killi (2014). The in situ measurements (including pseudo observations from satellite) are interpolated horizontally (from point measurements to a 2D field) based on distance dependent correlation functions with the optimal interpolation (OI) scheme (Brasnett, 1999). The snow water equivalent is finally inserted directly into the model replacing the background field. The snow analysis is not allowed to add snow on snow free grid cells if the surface temperature is above the melting-point of water.

2.2 Land surface model

For modelling the land surface, we use the ISBA model (Noilhan and Mahfouf, 1996; Calvet et al., 1998; Decharme et al., 2011) within the SURFEX framework (Masson et al., 2013). The ISBA model is set up using two patches (low and high vegetation), the multi-layer diffusion soil scheme (Decharme et al., 2011), explicit snow scheme (Decharme et al., 2016) and the explicit canopy option (Boone et al., 2017; Napoly et al., 2017) for the high vegetation patch. We have also adopted some of the configurations in Monteiro et al. (2024), including the reduced heat flux between soil and snow and the soil organic carbon dataset from soilgrids (Hengl et al., 2017). Using two patches means that within a grid cell, two independent mass and energy budgets are computed, adapted to the vegetation type. The resulting soil and snow states thus represent different sub grid conditions.

We use the ISBA explicit snow model with the default 12 layers, adding information about the vertical structure of the snow compared the the single layer model. The prognostic variables are snow water equivalent, snow density, snow heat content, albedo and snow age.

The land surface model is driven by atmospheric variables including precipitation (snow and rain), radiation (direct short-wave, diffuse shortwave and longwave), air temperature and humidity, surface pressure and wind. In this work, the forcing data is obtained from CARRA (Schyberg H. et al., 2021). The CARRA dataset has proven to perform better compared to the ERA5 product for both temperature and wind particularly in areas with complex topography (Køltzow et al., 2022; Box et al., 2023). The data is interpolated spatially to the model grid and SURFEX internally interpolates the hourly values to the 10 minute time step.

2.3 Data assimilation

Data assimilation aims to bring the model state closer to the true unknown state based on observations. The corrected state, called the analysis (a), can be expressed as the original state, often referred to as first guess, forecast or the background state (b), and a correction term,

$$\mathbf{x}^a = \mathbf{x}^b + \delta\mathbf{x} \tag{1}$$

here the correction ($\delta\mathbf{x}$), referred to as the increment, is typically a function of the innovation vector ($\mathbf{y}^o - \mathbf{y}^b$) where $\mathbf{y}^o$ represents the observations, and $\mathbf{y}^b = h(\mathbf{x}^b)$ is the model state in observation space, with h being a nonlinear observation operator.

According to Helmert et al. (2018), the most commonly used method for snow data assimilation in numerical weather prediction systems is the optimal interpolation (OI) method (e.g., Brasnett, 1999; Liston and Hiemstra, 2008; de Rosnay et al., 2014; Li et al., 2022). OI uses predefined structure functions to correlate observations with grid point values based on horizontal and vertical distances, often modelled with Gaussian curves (Gaspari and Cohn, 1999; Brasnett, 1999). When snow depth measurements are used to correct snow water equivalent and snow density, the solution is not unique. It is common practice to assume that the snow density is constant and only update the snow water equivalent (see references above). With more advanced snow models, like ISBA explicit snow, the state vector becomes significantly larger compared to single layer models. With a 12 layer configuration, the control vector consists of 36 prognostic variables at every grid point patch (snow water equivalent, snow density and snow heat, each times 12 layers). Distributing the analysis increments between all the different control variables can thus be challenging. However, so called flow dependent data assimilation schemes can objectively optimize the analysis state by taking the current conditions (errors of the day) into account and thus narrow down the possible solution space. The EnKF (Evensen, 2003) uses an ensemble of model realizations to represent the background error covariance matrix and it is widely used in snow data assimilation (Slater and Clark, 2006; Durand and Margulis, 2007; Lannoy et al., 2010; Kumar et al., 2017; Brangers et al., 2024). In the Kalman Filter, the increment is written

$$\delta\mathbf{x} = \mathbf{K}(\mathbf{y}^o - \mathbf{y}^b) \tag{2}$$

where $\mathbf{K}$ is called the Kalman gain matrix, and is defined as

$$\mathbf{K} = \mathbf{P}\mathbf{H}^T(\mathbf{H}\mathbf{P}\mathbf{H}^T + \mathbf{R})^{-1} \tag{3}$$

where $\mathbf{P}$ is the background error covariance matrix, $\mathbf{H}$ the linearized observation operator and $\mathbf{R}$ is the observation error covariance matrix. Furthermore, Lannoy et al. (2010) show that the EnKF gain matrix is written

$$\mathbf{K} = \text{cov}[\mathbf{x}, h(\mathbf{x})][\text{cov}[h(\mathbf{x}), h(\mathbf{x})] + \mathbf{R}]^{-1}. \tag{4}$$

Here, the error covariance matrices are not computed explicitly, but implicitly through the ensemble covariances.

In geophysical applications, the state vector has high dimensionality and large ensembles can be computationally expensive. Consequently, small ensembles have to be used and sampling noise is inevitable. The sampling noise could lead to spurious correlations between variables (Leutbecher, 2019). Essentially, the spurious correlations result in increments based on unrealistic relationships between the observation and the control vector. This behaviour is avoided by limiting the impact of observations outside their representative area, referred to as localization. Localization can be applied by tapering the background covariance matrix, or by so called local analysis (Sakov and Bertino, 2011).

Hunt et al. (2007) proposed a localized version of the EnKF, solving the filter equations individually at each grid point. Due to the manageable use of computational resources and the flexibility regarding observation types, we have chosen their implementation of the local ensemble transform Kalman filter (LETKF). The LETKF has shown promising results in both atmospheric and surface data assimilation systems (Shin et al., 2016; Gastaldo et al., 2018; Seo et al., 2021; Nerger, 2022; Lee

et al., 2024). The LETKF update equations are:

$$\mathbf{x}^a = \bar{\mathbf{x}}^b + \mathbf{X}^b \mathbf{w}^a$$

155
$$\mathbf{w}^a = \mathbf{W}^a + \bar{\mathbf{w}}^a$$

$$\bar{\mathbf{w}}^a = \tilde{\mathbf{P}}^a (\mathbf{Y}^b)^T \mathbf{R}^{-1} (\mathbf{y}^o - \bar{\mathbf{y}}^b)$$

$$\mathbf{W}^a = [(k-1)\tilde{\mathbf{P}}^a]^{1/2}$$

$$\tilde{\mathbf{P}}^a = [(k-1)\beta^{-1}\mathbf{I} + (\alpha \circ (\mathbf{Y}^b)^T \mathbf{R}^{-1})\mathbf{Y}^b]^{-1}$$

where $\mathbf{x}$ represents the ensemble control vector, $\mathbf{X} = \mathbf{x} - \bar{\mathbf{x}}$ the ensemble anomalies (or perturbations), bar represents ensemble-

160 mean, a and b indicate analysis and background respectively, $\mathbf{w}$ is the transformation weights between the background and the

analysis, $\mathbf{Y}^\mathbf{b}$ represent the ensemble perturbations of the observation equivalent. $\tilde{\mathbf{P}}$ and $\mathbf{R}$ are the error covariance matrices. β

and α are tunable parameters for inflating the background error covariance matrix and to apply localization (inflation of $\mathbf{R}$),

respectively.

To compute the model state in observation space, we use the following observation operator:

165
$$y^b = h(\mathbf{x}^b) = \sum_i^2 \sum_j^{12} \gamma_i \frac{w^b_{i,j}}{\rho^b_{i,j}} \tag{5}$$

where w and ρ represent the snow water equivalent and snow density respectively and γ_i is the patch (open land or forest)

fraction. The counter i represent the model patch and j the snow model level.

As shown in Diefenbach et al. (2023), the analysis equation for the ensemble-mean $\bar{\mathbf{x}}^a$ can be written as

$$\bar{\mathbf{x}}^a = \bar{\mathbf{x}}^b + (k-1)^{-1}\mathbf{X}^a \mathbf{Y}^{aT} \mathbf{R}^{-1} (\mathbf{y}^o - \bar{\mathbf{y}}^b). \tag{6}$$

170 This is the common form of the Kalman Filter where $(k-1)^{-1}\mathbf{X}^a \mathbf{Y}^a \mathbf{R}^{-1}$ corresponds to the gain matrix $\mathbf{K}$ mapping the

innovations $(\mathbf{y}^o - \bar{\mathbf{y}}^b)$ in observation space to increments $(\mathbf{x}^a - \mathbf{x}^b)$ in model space. Investigating the elements of $\mathbf{K}$ is important

for understanding the filter performance. We recognize that $\mathbf{X}^a \mathbf{Y}^{aT}$ is proportional to the ensemble correlation between the

model space state and the observation space state. The ensemble correlation between a model variable (i) and an observed

quantity (j) is given by

175
$$r_{ij} = \frac{\mathbf{X}^i \mathbf{Y}^{jT}}{\sqrt{\mathbf{X}^i \mathbf{X}^{iT} + \mathbf{Y}^j \mathbf{Y}^{jT}}}. \tag{7}$$

2.4 Ensemble perturbations

For ensemble based data assimilation methods, the ensemble perturbations $\mathbf{X}$ and $\mathbf{Y}$ are used to represent the uncertainty

of the model estimate. They also describe the relationships between locations and between variables which map innovations

to increments as shown above. It thus require care when generating the ensemble to ensure realistic relationship between the

180 variables. The uncertainty can be sampled by perturbing forcing data, model state variables, model parameters or a combination

of these (Slater and Clark, 2006; Lannoy et al., 2010; Liu et al., 2011; Kumar et al., 2014, 2017; Blyverket et al., 2019; Draper,

2021; Seo et al., 2021; Brangers et al., 2024). The benefit of only perturbing the forcing data is that the resulting model states are consistent with the model physics and the relationship between variables is as realistic as the model. However, processes that are unresolved by the model, for example redistribution by wind in our model, will not be represented by the ensemble

185 by only perturbing the forcing data. Since we in this work introduce a large control vector relative to the observation vector, we only perturb the forcing data (rain, snow, longwave radiation, shortwave radiation, air temperature) to reduce the chance of introducing sampling noise. We follow the above studies and use cross-correlation between forcing variables to ensure realistic forcing conditions, temporal auto-correlation of the noise and spatially correlated noise (Reichle and Koster, 2003; Durand and Margulis, 2007; Lannoy et al., 2010).

190 Precipitation forcing is usually perturbed by multiplying the field with noise from a log-normal distribution to avoid positive precipitation bias in the case of no precipitation (see references above). This method is not able to represent the possibility of precipitation if the original dataset has zero precipitation. Maggioni et al. (2012) used an advanced error model for satellite precipitation products to approach this issue with good results on soil moisture fields. However, it requires calibration with satellite and a radar reference which is not generally available. In this work we introduce a novel approach to improve the

195 spatial representation of precipitation uncertainty. By assuming that precipitation fields in the forcing data have an error in horizontal placement, we can introduce uncertainty in areas surrounding such fields. We refer to the method as remapping and is based on advection using a random vector field. The approach builds on ideas from Le Coz et al. (2019), where precipitation fields are remapped to better fit observations. An illustrative example of the remapping method is shown in Fig. 1. The figure demonstrates how a grid point with no precipitation in the original forcing data can be updated by the assimilation scheme when

200 the remapping is used. Given that the marked point is an observation and the observation indicates too little snow in the model, the areas with positive/negative ensemble correlations would add/remove snow. Due to the strong forcing from orography on precipitation, we reduced the advection vectors in areas with complex terrain. A detailed formulation of the method is found in Appendix A.

2.5 Conditioning of ensemble states

205 In the SURFEX model, snow water equivalent is defined in all model points. In grid points with no snow, the snow water equivalent is zero and the other prognostic variables (density, age, albedo and heat) are undefined. In order to include these grid points in the analysis and potentially add snow to snow free members, undefined values need to be initialized. While some predefined values can be used, e.g. corresponding to freshly fallen snow, such simplifications can quickly introduce nonlinear relationships between ensemble members. For example, during melting season, one member becomes snow free while the

210 other members still have old and very dense snow. A different approach is to use a sample from the members containing snow to initialize zero snow members. Even though this method might not produce a representative spread for the snow, it avoids the filter to produce unrealistic analyses. In this work we initialized zero snow members with the ensemble-mean of members with snow. If all members are snow free, the filter is unable to add snow.

After the data assimilation is performed, the analysed state is the best estimate given that the assumptions of the filter

215 hold. However, it might not be physically consistent, nor within the model bounds. The result can thus cause instabilities in
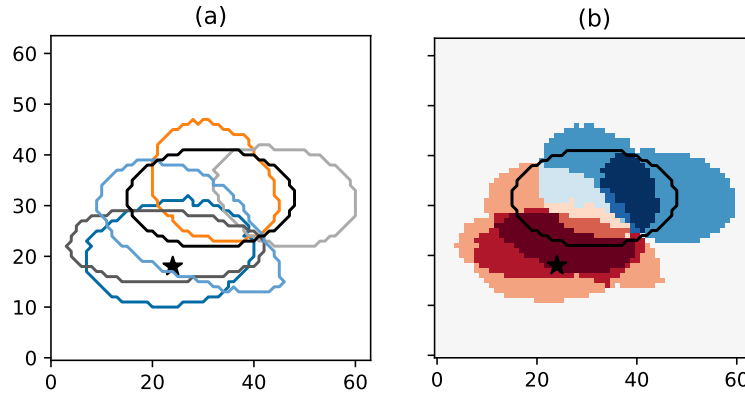
Figure 1. Illustration of remapping. (a) shows original field (e.g. snow fall) in black contour line, the other colours indicate ensemble members after remapping. (b) shows ensemble correlations between the point indicated by a star and the respective surrounding grid points.

Table 1. Valid ranges for snowpack quantities

snow water equivalent w	$0 \leq w$
snow density ρ	$50 \leq \rho \leq 917.3$
snow temperature (diagnostic) T	$200 \leq T$
snow heat h	$h < 0$

the preceding model integration and result in a model crash. For example, negative snow water equivalent can occur in the analysed state. In the data assimilation system, we use the ensemble-mean approach as mentioned above given that a member exceeds any of the limits in Table 1. This method prioritizes stability of the model integration over optimal performance of the filter.

220 ## 2.6 Validation and observation data

In situ snow depth observations used in the data assimilation is obtained from the Meteorological Archival and Retrieval System (MARS) of the European Centre for Medium-Range Weather Forecasts (ECMWF). The observation dataset is not identical to the one used in CARRA, as CARRA uses additional local observations and a different quality control. Thus, we can bin observations into three sets. Let $\hat{A}$ be the observations used in CARRA-Land-Pv1 and $\hat{B}$ the observations used in CARRA.

Table 2. Observation sets with corresponding acronyms, total number of stations and total number of observations during the experiment period

Set	Assimilated in	Acronym	num. stations	num. observations
A	CARRA-Land-Pv1	OBS-ONLY-Pv1	178	122590
B	CARRA	OBS-ONLY-CARRA	111	108652
C	CARRA and CARRA-Land-Pv1	OBS-BOTH	144	124416
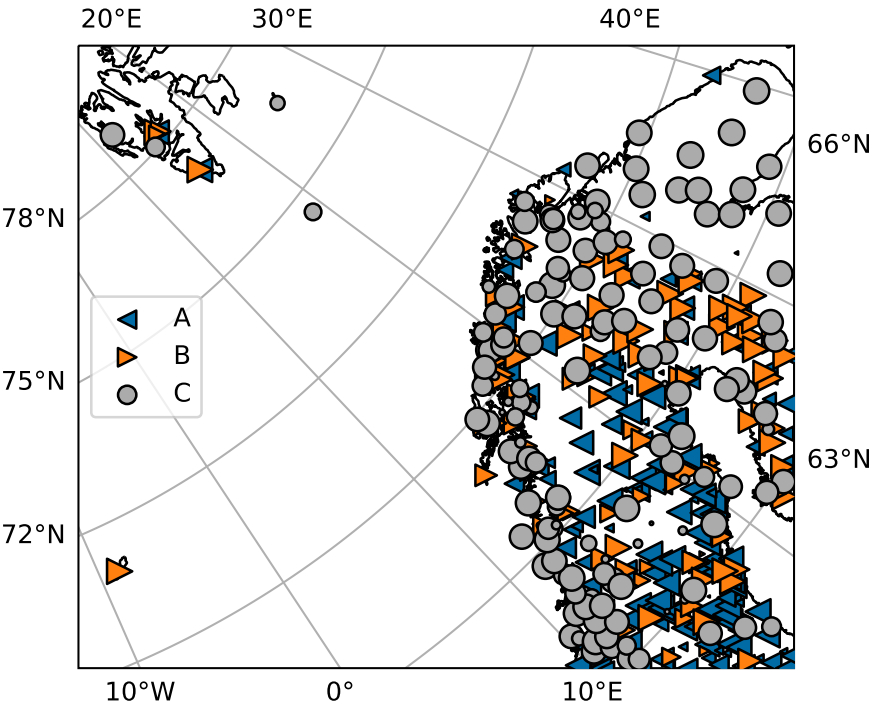
Figure 2. Observations of snow depth only used in CARRA-Land-Pv1 (set A), only in CARRA (set B) and in both (set C). Marker size indicates the number of observations through the study period.

225   Further let $C = \hat{A} \cap \hat{B}$ be the observations used in both systems, $A = \hat{A} - \hat{B}$ the stations only used in CARRA-Land-Pv1 and $B = \hat{B} - \hat{A}$ the stations only used in CARRA. In the following we will denote dataset A as "OBS-ONLY-Pv1", B as "OBS-ONLY-CARRA" and C as "OBS-BOTH". In addition, snow water equivalent from 6 snow pillow stations (Tollan, 1970; Egli et al., 2009) are used to evaluate the unobserved (by the assimilation system) snow water equivalent state.

2.7 Experimental setup

230   Our experiments are set up on the eastern domain of the CARRA product, covering northern Scandinavia and Svalbard. The simulations are initialized on 1 September 2015 and cover the next four consecutive winters. Snow data assimilation is

performed daily at 06 UTC using in situ snow depth measurements. In line with Yin et al. (2015); Brangers et al. (2024) and references therein, the number of ensemble members was chosen after comparing shorter experiments with different ensemble sizes. Compared to using 20 members, a 10-member ensemble gave no considerable degradation in performance.

235 Additionally, an unperturbed control member was run without data assimilation for validation purposes. Hereafter, we refer to the unperturbed run as CTRL and the analysed ensemble simulation as CARRA-Land-Pv1 (Prototype version 1). The purpose of CARRA-Land-Pv1 is to provide a more realistic dataset of the snowpack covering the region.

3 Results

In this section, we present the evaluation of the CARRA-Land-Pv1 dataset covering 1 November 2015 to 1 August 2019.

240 First, in Sect. 3.1 we show diagnostics of the data assimilation system, including average analysis increments and ensemble correlations. Subsequently, we present the evaluation of the resulting snow depth dataset (Sect. 3.2) and validation against in situ observations compared to CARRA and CTRL (Sect. 3.3). Finally, in Sect. 3.4 we present a verification of modelled snow water equivalent versus snow pillow observations.

3.1 Data assimilation diagnostics

245 We focus on vertically aggregated values, summarizing the values in the 12 layers of the model and define

$$d_{tot} = \sum_i^{12} d_i \qquad w_{tot} = \sum_i^{12} w_i \qquad \rho_{tot} = \frac{w_{tot}}{d_{tot}} \qquad (8)$$

for snow depth, snow water equivalent and snow density respectively, where i indicates the model layer of the snow. The increments presented below are computed from the aggregated variables. For example, the total snow depth increment is written $\delta d_{tot} = d_{tot}^a - d_{tot}^b$, where a denote analysis and b denote background.

250 Figure 3 shows maps of the time averaged increments for snow depth δd_{tot} (a), snow water equivalent δw_{tot} (b) and snow density $\delta \rho_{tot}$ (c). Snow depth and snow water equivalent increments are consistently positive over the domain, while snow density increments are mainly negative. The magnitude of snow depth increments corresponds to several millimetres each day which roughly accumulates to a metre over one year. For snow water equivalent, about 200 mm of water is added each year through the increments. The time averaged snow depth innovations $\overline{(y^o - \bar{y}^b)}$ are shown together with the average snow depth

255 increments (Fig. 3 a). Some observation sites are surrounded by increments with non-zero mean, particularly in the inland areas. The patterns of these increments are similar to the Gaussian localization function. The systematic positive increments are related to positive innovations, indicating too little snow in the model. Similar patterns but with opposite sign are not seen around stations with negative innovations (indicating too much snow in the model). The stations with mean negative innovations are situated in mountainous areas and have small impact on the analysis. This is due too the large vertical distance

260 between model and observation and thus the increment is dampened by the localization (not shown).

Time series of domain averaged increments are shown in Fig. 4 for the same variables as Fig. 3. Largest positive snow depth increments are seen during spring where snow water equivalent increments are positive and density increments are negative.
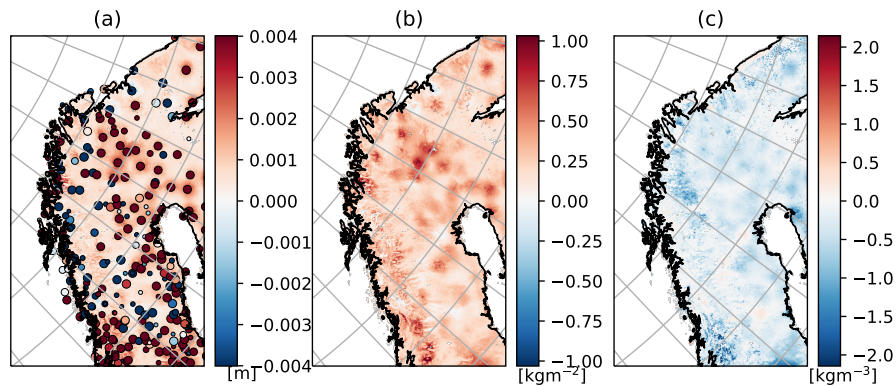
Figure 3. Mean (time average) increments of (a) total snow depth (δd_{tot}), (b) snow water equivalent (δw_{tot}) and (c) snow density ($\delta \rho_{tot}$). Dots in (a) indicate mean innovation at assimilated observations and their size indicates the number of observations.
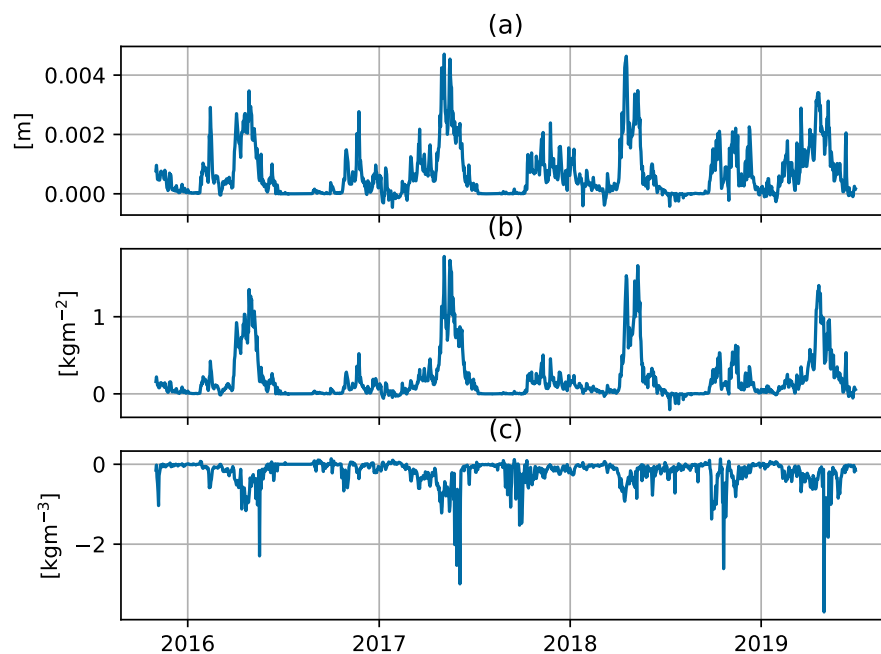
Figure 4. Mean (domain average) increments of (a) total snow depth (δd_{tot}), (b) snow water equivalent δw_{tot} and (c) snow density ($\delta \rho_{tot}$).
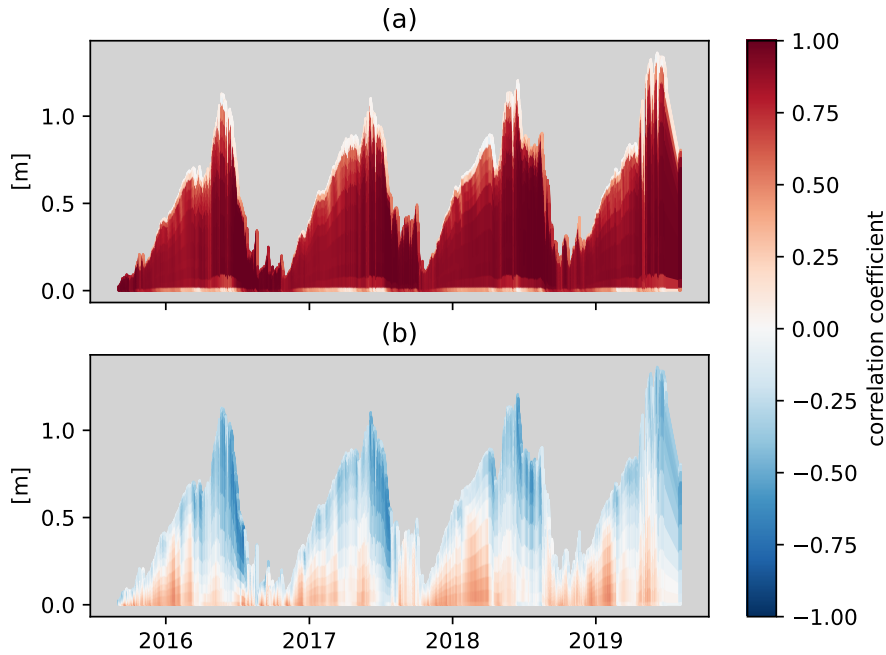
Figure 5. Time series of domain average snow depth d_{tot} with colour-contoured ensemble correlations between total snow depth d_{tot} and snow water equivalent w_i (a) and between d_{tot} and snow density ρ_i (b) per model level using Eq. 7. Only grid points with snow are used, thus the depth is only representative for snow covered grid cells.

The early accumulation phase is also dominated by positive snow depth increments, but with smaller density increments. During the winter, snow depth increments decrease and in some years they become slightly negative before the melting phase

265   begins. The figure suggests that snow is melting (loosing mass and compacting) too rapidly during spring, and that there is a slight underestimation of snowfall in the early accumulation phase.

We continue by investigating the structures of the Kalman gain matrix **K** through the ensemble correlations according to Eq. 7. Figure 5 presents snow profile time series with ensemble correlations between observation and model variables. Large positive correlations, as seen for snow water equivalent, indicate that a positive innovation (model snow depth is too small)

270   will cause a positive increment to the control variable (increasing snow water equivalent). For snow density (Fig. 4b), there is a positive correlation between snow depth and density in the lower layers during accumulation. This can be explained by the compaction of the lower layers in the snowpack due to increased mass in the upper layers during snowfall. The upper layers have negative correlations and strongest in the melting phase. Given a positive innovation in snow depth, the negative correlations would cause the analysis to decrease the density (increase snow depth) to compensate for too high compaction

275   in the model simulation. The introduction of density in the control vector allows the snow depth to be adjusted 1) without changing the snow mass (negative correlations between total snow depth and snow density) and 2) larger change in snow mass compared to only updating mass in the case of positive density correlation.
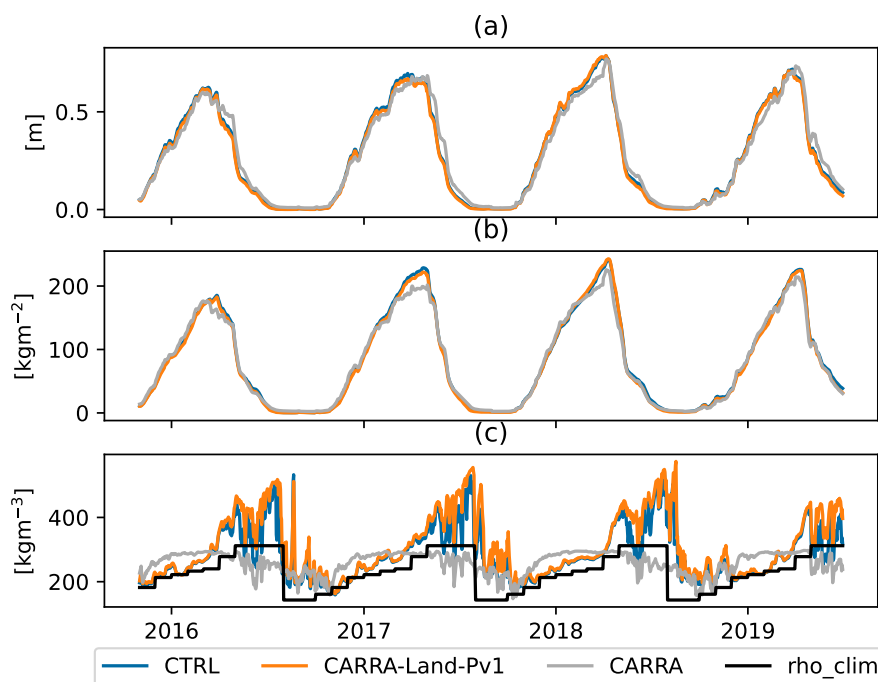
Figure 6. Time series of domain average: total snow depth d_{tot} (a), snow water equivalent w_{tot} (b) and snow density ρ_{tot} (c) for CTRL (blue), CARRA-Land-Pv1 (orange) and CARRA (green). Black line indicates climatological snow densities used for converting observations to snow water equivalent in the CARRA system

3.2 Seasonal snow characteristics

Figure 6 shows the evolution of domain average snow depth (a), snow water equivalent (b) and snow density (c) for the
280   CARRA-Land-Pv1, CTRL and CARRA. In terms of snow water equivalent, CTRL and CARRA-Land-Pv1 have higher values
at the yearly maximum compared to CARRA. In general, there are relatively small differences between CARRA-Land-Pv1 and
CTRL. In CTRL and CARRA-Land-Pv1 the evolution of snow water equivalent is smoother compared to CARRA. CARRA
tends to have lower snow depth than CARRA-Land-Pv1 and CTRL during the accumulation phase and higher during the melt
phase. These characteristics are consistent for all years. The density evolves quite differently in the two snow models (CARRA
285   vs CTRL and CARRA-Land-Pv1). In the single layer snow scheme used in CARRA, the maximum snow density is $300\ \mathrm{kgm^{-3}}$
while the explicit snow scheme (CTRL and CARRA-Land-Pv1) has an upper limit at $973\ \mathrm{kgm^{-3}}$. The snow density reach high
values in the melting phase in the multi-layer snow scheme. In CARRA, snow density is increasing faster in the accumulation
phase, and stabilises earlier in the winter. During the melting phase the snow density in CARRA decreases compared to the
density in the multi-layer models. There is a discrepancy between the CARRA snow density and the climatological values used
290   in its snow analysis. On average, this climatological density is less than the CARRA density before April and greater after
May. This coincides with the snow depth differences described above.
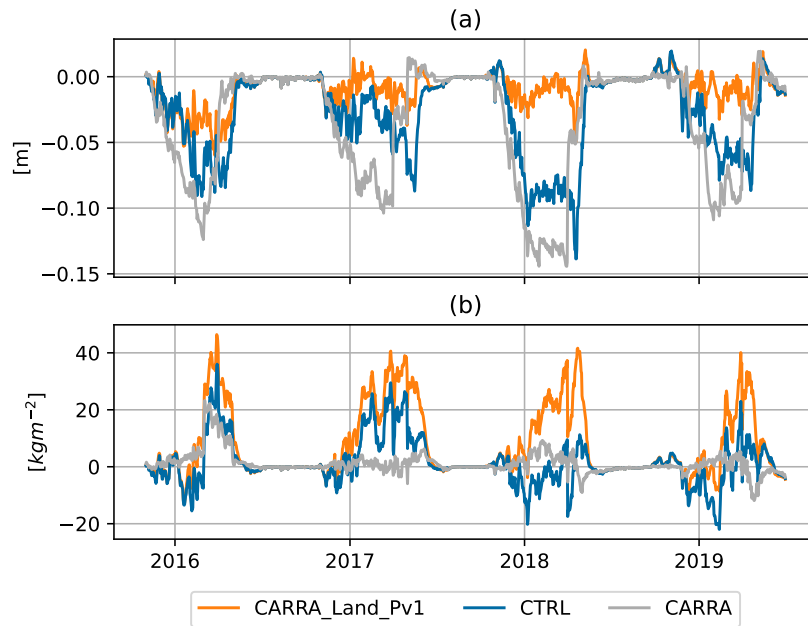
Figure 7. Differences between model and observation snow depth d_{tot} (a) and snow water equivalent w_{tot} (b) averaged over all observation locations. (b) shows difference between model and observations converted to snow water equivalent using climatological densities.

Time series of mean errors in total snow depth and snow water equivalent averaged over all observation sites are shown in Fig. 7. All datasets have negative bias in snow depth and the largest bias is seen in CARRA. CARRA-Land-Pv1 has smallest negative bias indicating larger snow depth compared to both CARRA and CTRL. For snow water equivalent, CARRA has

295   smaller differences. Note that CARRA assimilates snow water equivalent and not snow depth. However, the conversion is not accurate and the resulting snow depth is systematically underestimated.

3.3 Snow depth validation

Time series of continuous rank probability score (CRPS) (for ensemble) and mean absolute error (MAE) (for deterministic) over the three different observational sets are shown in Fig. 8 and Table 2. Largest errors are seen for CTRL in all sets and

300   yearly maximum varies between 15 and 30 cm. Comparing the three observation sets, the largest errors overall are in OBS-ONLY-CARRA. CARRA has larger errors than CARRA-Land-Pv1 in OBS-ONLY-Pv1 and OBS-BOTH, with values ranging from 10 to 20 cm and 5 to 10 cm respectively. For CARRA-Land-Pv1 a degradation is seen for OBS-ONLY-CARRA but it is consistently better than CTRL. We also note a significant drop in errors in CARRA during spring, this is seen for all years. This drop coincides with the transition from March to April and thus new values for climatological density used in CARRAs

305   snow data assimilation From Fig. 6 (c), April is the month where the climatological densities fit best with the model density in CARRA.
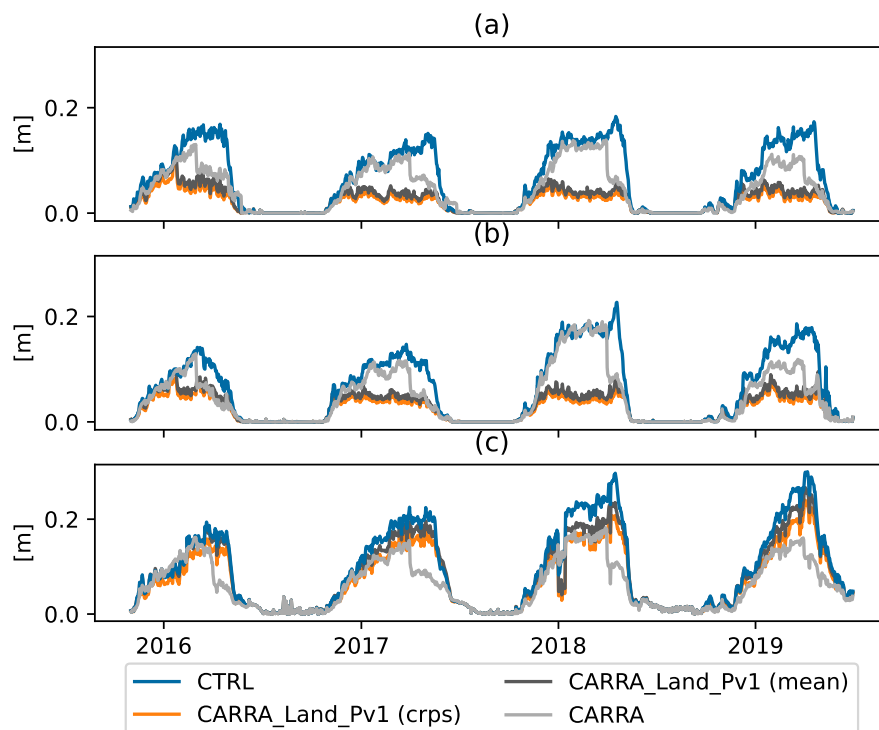
Figure 8. Time series of CRPS (for CARRA-Land-Pv1 ensemble) and MAE (for deterministic products) for three different observational sets. (a) shows scores based on OBS-BOTH, (b) OBS-ONLY-Pv1 and (c) OBS-ONLY-CARRA

We have included both CRPS and MAE of the ensemble-mean to highlight the benefit of CARRA-Land-Pv1 being an ensemble product. The CRPS values are consistently lower than the MAE of the ensemble-mean. However, relative to the other datasets, the CRPS and MAE of ensemble-mean are quite close. When CRPS for CARRA-Land-Pv1 and MAE of the
310   other products are compared, the advantage of using the ensemble is only marginally contributing to the differences.

Maps of the difference in CRPS between CARRA-Land-Pv1 and CARRA for the three observation sets are shown in Fig. 9. For the stations in OBS-BOTH (a) and OBS-ONLY-Pv1 (b), CARRA-Land-Pv1 performs better than CARRA/CTRL (CTRL not shown) for most station points. This is also the case for the OBS-ONLY-CARRA set (c), except for a number of stations along the Norwegian mountains and a few scattered inland stations. A closer investigation of the points where CARRA has
315   smaller errors, reveals the following characteristics. 1) The station is isolated, through the localization, from other stations, 2) the point is close to another (assimilated) station with different climatology. In one case we found up to 50 cm difference in snow depth between observations at neighbouring grid points (not shown). We also note that the spatial distribution of observations in each set differs. In OBS-ONLY-Pv1, more observations are found in the southern part of the domain compared to OBS-ONLY-CARRA.
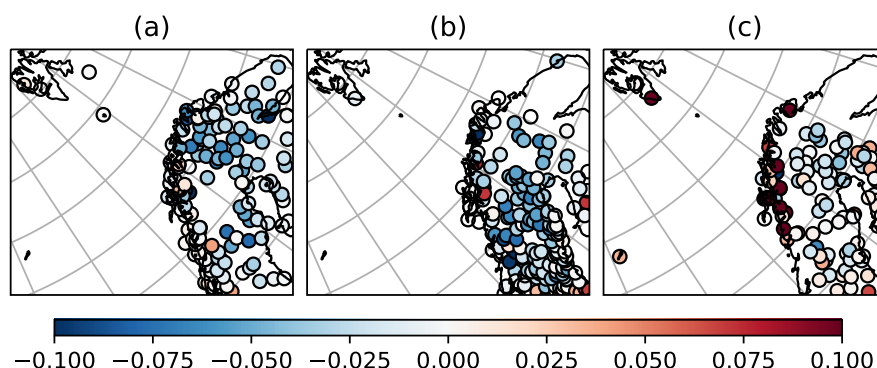
Figure 9. Difference in CRPS/MAE scores (CARRA-Land-Pv1 minus CARRA) averaged over time for each observation site. Blue colour indicates smaller errors in CARRA-Land-Pv1 Panels corresponds to observation sets OBS-BOTH (a), OBS-ONLY-Pv1 (b), OBS-ONLY-CARRA (c).

Table 3. Summary statistics for the different datasets. Each cell contains values for the three observation sets (OBS-BOTH/OBS-ONLY-Pv1/OBS-ONLY-CARRA). Relative improvements are shown in the two rightmost columns as 100(ref - CARRA-Land-Pv1)/ref

	CARRA	CTRL	CARRA-Land-Pv1	rel CARRA (%)	rel CTRL (%)
CRPS/MAE	0.05 / 0.05 / 0.06	0.06 / 0.06 / 0.09	0.02 / 0.03 / 0.07	52.68 / 47.85 / -20.79	66.53 / 59.57 / 21.53
Bias	-0.03 / -0.04 / -0.04	-0.03 / -0.03 / -0.01	-0.01 / -0.01 / -0.01	78.11 / 70.31 / 85.15	76.83 / 63.25 / 51.15
Stderr	0.08 / 0.08 / 0.14	0.12 / 0.11 / 0.22	0.05 / 0.07 / 0.20	32.14 / 15.14 / -46.50	55.34 / 42.53 / 6.09
Corr	0.96 / 0.98 / 0.92	0.89 / 0.92 / 0.81	0.98 / 0.98 / 0.83	-2.22 / -0.41 / 9.93	-9.64 / -5.93 / -2.63

320   Summary scores are presented in Table 3. Compared to CTRL, CARRA-Land-Pv1 improves on all scores in all observation sets. Relative to CARRA, scores are worse over OBS-ONLY-CARRA, except for bias which is improved by 85%. Over OBS-ONLY-Pv1 and OBS-BOTH, CARRA-Land-Pv1 performs better than the other datasets.

3.4 Snow water equivalent validation

In the following comparison, we compute the MAE between CTRL, CARRA and CARRA-Land-Pv1 (ensemble-mean) and the
325   six snow water equivalent observations available over the domain. Figure 10 shows differences in MAE (CARRA-Land-Pv1 minus CTRL (a) and CARRA-Land-Pv1 minus CARRA (b)) for each station. The dots indicate that snow water equivalent is improved through snow depth data assimilation in four stations and has neutral impact in two. Compared to CARRA, CARRA-Land-Pv1 has improved snow water equivalent in three, neutral in two and degraded in one station. The areas surrounding the stations with reduced errors compared to CARRA are associated with larger snow water equivalent values. The degraded station
330   is on the other hand surrounded by negative snow water equivalent differences. In inland areas, the snow water equivalent differences are smaller in magnitude, but mostly positive.
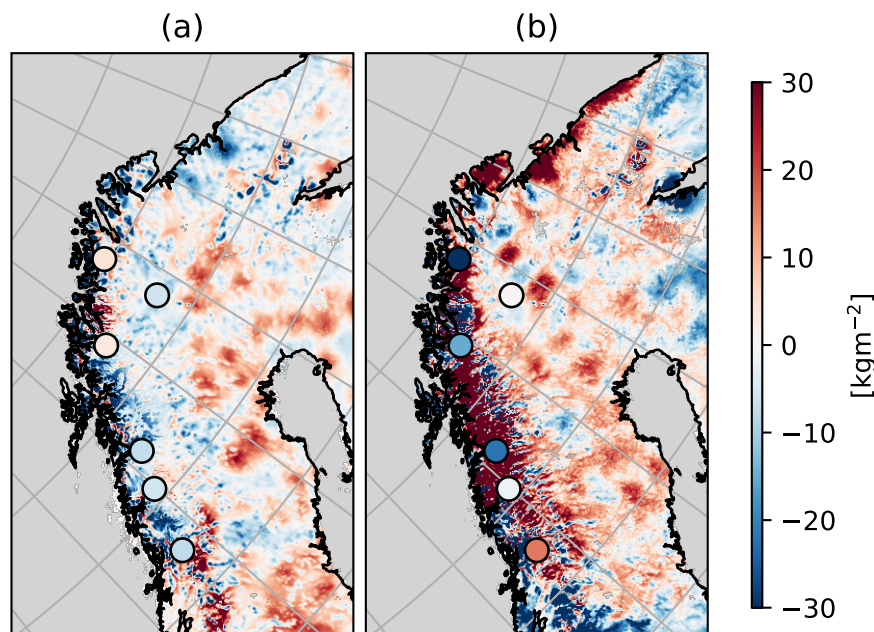
Figure 10. Dots representing difference between MAE of CARRA-Land-Pv1 ensemble-mean and references. The references are CTRL (a) and CARRA (b). The MAE is computed from modelled total snow water equivalent w_{tot} and observed snow water equivalent from snow pillow observations. Blue dots indicate smaller absolute errors in CARRA-Land-Pv1 compared to the reference experiment. Colour-shading represents the mean difference in snow water equivalent between the experiments.

4 Discussion

Our evaluation of the new regional land reanalysis system (CARRA-Land-Pv1) shows promising results with reduced errors of snow depth estimates compared to CARRA and CTRL. The multi-layer snow scheme also shows the ability to accumulate

335 more mass within the snowpack during the winter, with about 10% more than CARRA at maximum snow depth. Additionally, the data assimilation scheme adds substantial amounts of snow compared to CTRL. The multi-layer scheme allows for much higher snow density during the melting phase, however, this is slightly moderated by the data assimilation increments (negative increments in density). The time series of mean analysis increments (Fig. 4) indicates systematic errors during spring. The snow depth errors in CTRL are also largest during this period. This suggests a limitation in the model parametrization for melting,

340 or an underestimation of precipitation in the CARRA forcing. A similar underestimation of snow depth is also seen in the CARRA dataset, strengthening the latter suspicion. Significant improvements due to model configuration was obtained by Monteiro et al. (2024) related to the melting season. Adopting all their settings will be considered in future work.

Investigation of the ensemble correlations (Fig. 5), indirectly by the Kalman gain matrix, gives insight in how the snow depth observations are used to update the relatively large control vector. The relationship between total snow depth and snow water

345 equivalent is almost one to one. This indicates that the common approach in the literature to only update snow water equivalent

in snow data assimilation systems is efficient and reasonable, also for multi-layer schemes. However, the ensemble correlation between total snow depth and snow density indicates important contributions from snow density. Two main processes are represented by the correlations: 1) compaction during accumulation and 2) compaction due to melting. These correspond to positive and negative correlations between total snow depth and snow density respectively. The first in lower layers and the latter in the upper layers.

Unfortunately, collocated observations of snow depth, snow water equivalent and snow density are (to our knowledge) not available in our study area. The few snow water equivalent observations show mixed results, but indicate an overall positive impact of the system. We emphasize that these stations are not collocated with assimilated snow depth observations. Since snow depth is generally improved, the uncertainty of snow water equivalent lies mainly in the snow density. Our investigation of ensemble correlations suggests that the assimilation scheme is able to produce realistic corrections also to density. In studies where more snow water equivalent measurements for validation was available, comparable ensemble-based data assimilation systems gave improved snow water equivalent estimates (Magnusson et al., 2017; Smyth et al., 2020).

By exploring the different observation sets used in CARRA and CARRA-Land-Pv1, we evaluate the analysis performance where observations are not available for assimilation. Despite that CARRA-Land-Pv1 performs worse than CARRA over OBS-ONLY-CARRA, errors are consistently reduced compared to CTRL for these stations. These findings are in line with results in Oberrauch et al. (2024). Nevertheless, the distance based localization used in CARRA-Land-Pv1 cause several stations in OBS-ONLY-CARRA to be unreachable in the analysis. Cluzet et al. (2022) evaluated different localization strategies for in situ snow depth measurements in mountain regions and found that using ensemble correlation between variables at different grid points rather than distance to localize the analysis was beneficial. Such method should also be evaluated for our system and study area. Although smaller improvements are seen over mountain areas for CARRA-Land-Pv1 comparing to in situ observations, the topography has strong impact on precipitation. This suggests that also the uncertainties should be modified in these areas. We account for topography in the precipitation remapping, but not in the spatial structure of the other noise fields perturbing the amplitudes. We thus suggest that more work is needed to improve the quality of spatial structures for the forcing ensemble.

In this study we used the model grid average snow depth as observation equivalent. However, we found cases where observations close to each other had very different snow depths, which indicates large sub-grid variability. There are also potentially systematic differences in snow conditions between the low and high vegetation patches, and, likely, the observation is not representative of the grid average value. This deficiency could also explain the systematic increments during melting phase as discussed above. For example, in a grid cell represented by 50% low and 50% high vegetation, a snow depth observation reads 40 cm. Furthermore, in the high vegetation (forest) patch of the model, the snow is gone, while in the low vegetation patch (where most snow observations are located) the model has 50 cm of snow. Using the grid average observation operator will give an observation equivalent of 25 cm resulting in an innovation of 15 cm. Consequently, this will typically cause snow to be added. However, given that the observation is representative of an open area, we could use the low vegetation patch only to compute the observation equivalent which results in a negative innovation of -10 cm, and snow will be removed. Another important case is areas where snow is redistributed by wind (Gisnås et al., 2016; Aas et al., 2017). This process is not represented

in the ISBA explicit snow model, however if accounted for in the observation operator the observations can still be used to correct the model values. In emission modelling, the use of statistical models for subgrid processes has been used to encounter similar problems (Koohkan and Bocquet, 2012).

385   A fundamental difference between CARRA and CARRA-Land-Pv1 systems is the flow dependency of the ensemble-based CARRA-Land-Pv1 versus the static CARRA assimilation scheme. Where the CARRA system will treat any value of an observation equally, but CARRA-Land-Pv1 will account for the background uncertainties. For instance, if all members are snow-free, no observation of snow depth results in non-zero increments. This has potential weaknesses, however, as long as the ensemble has reliable uncertainties it can prevent unwanted increments due to erroneous observations. Although not presented, we found several cases of inconsistencies within the CARRA dataset. On the other hand, the CARRA-Land-Pv1 shows more

390   consistent time series and spatial patterns. Due to more confidence in the model background, single observations have less impact. However, we have seen that small increments over time ensures that the estimates follow observations closely.

5   Conclusions

In this study, we have implement a system for regional land reanalysis with enhanced representation of snow processes through a multi-layer snow scheme and the ensemble-based LETKF for data assimilation. A 4-year dataset is produced with the system

395   assimilating in situ snow depth observations. The dataset is evaluated and compared to existing products covering the European Arctic. The snow depth estimates showed reduced errors compared to the reference datasets and consistent positive impact of the data assimilation. However, limited impact is found in mountain regions along the Norwegian coast, which highlights fundamental challenges of snow modelling and assimilation in these regions.

    Through perturbation of forcing data, the ensemble is able to represent uncertainty related to compaction processes. This

400   allows the data assimilation to make corrections to the state variables accounting for these processes which are usually neglected when only snow water equivalent is updated.

    Systematic positive snow depth increments during spring are discussed and model parametrization and precipitation bias in the forcing data are highlighted as possible explanations. However, both of these deficiencies are corrected by the assimilation. Conversely, the representativeness errors of the observations are found to be large and, in some cases, impact the assimilation

405   performance negatively. We thus suggest future studies to develop more advanced observation operators for in situ snow measurements accounting for sub grid conditions (e.g. following Koohkan and Bocquet, 2012).

    For seasonal stream flow predictions, accurate estimates of snow water equivalent are crucial (Casson et al., 2018). The multi-layer surface scheme shows up to 10% difference in accumulated snow water during the maximum snow depth compared to CARRA. Moreover, the dataset shows less jumpy time series of snow water equivalent and its errors. This suggests that there

410   is a potential impact on downstream usage of this product, with more reliable estimates of snow water equivalent through the snow season.

    While the assimilation of in situ snow depth observations gives an overall positive impact, the spatial coverage is a limitation of these observations. To provide the best snow estimates covering all parts of the domain, more observations need to be

assimilated. Satellite based instruments operating in both visual and microwave frequencies have shown to provide accurate

415 estimates of different snow quantities (De Lannoy et al., 2012; de Rosnay et al., 2014; Charrois et al., 2016; Micheletty et al., 2022; Gichamo and Draper, 2022). With relatively frequent revisit times at high latitudes, these are attractive sources of information. Including new types of observations requires the implementation of an observation operator. For satellite observations, this can either be radiative transfer models like the Snow Microwave Radiative Transfer (SMRT) (Picard et al., 2018) or machine learning based observation operators (Kwon et al., 2019).

420 The system presented is also flexible in terms of extending the analyses to more than snow state. Herbert et al. (2024) demonstrated the benefit of unified surface data assimilation. The system used in this work is well suited for combining soil and snow data assimilation in a unified approach.

Data availability. Snow depth observations used in this study are obtained from the Meteorological Archival and Retrieval System (MARS) of the European Centre for Medium-Range Weather Forecasts (ECMWF) (restricted access). The Snow pillow observations were fetched

425 from the Hydrological API (HydAPI) provided by the Norwegian Water Resources and Energy Directorate (NVE) hydapi.nve.no. CARRA data is available from the Climate Data Store (CDS) (Schyberg H. et al., 2021). The CARRA-Land-Pv1 dataset is available from the corresponding author upon reasonable request.

Appendix A: Appendix

In the following, the remapping procedure is described step by step.

430 1. Construct a spatial correlated vector field $\mathbf{v}$. In this study, a 2D convolution with a Gaussian kernel function was used to obtain spatial correlations of a 2D random variable.

2. Let the vector $\mathbf{I}$ be the grid indices of the domain, mapping $P \rightarrow P$. Here P is the field to be remapped.

3. Advect $\mathbf{I}$ by $\mathbf{v}$ to obtain $\mathbf{I}'$

$$\mathbf{I}' = \mathbf{I} - \mathbf{v} \cdot \nabla I \tag{A1}$$

435 4. Compute P' by bilinear interpolation of $P(\mathbf{I}')$

$$P'_{i,j} = (1-\alpha)[\beta P_{i^-,j^+} + (1-\beta)P_{i^-,j^-}] \qquad + \alpha[\beta P_{i^+,j^+} + (1-\beta)P_{i^+,j^-}], \tag{A2}$$

where $\alpha = i' - i^-$, $\beta = j' - j^-$, the superscripts $-\prime$ and $+\prime$ indicate the advected index i' rounded down and up to closes integer respectively.

Since precipitation has moved within the domain, the phase might have changed and a redistribution of snow and rain is

440 necessary. If a grid cell have precipitation before the remapping, the original ratio r between snow and total precipitation is used. However, if it does not exist (total precipitation was zero), the forcing temperature T is used as

$$r = \begin{cases} 1 \text{ if } T \leq 272 \\ 1 - \frac{T-272}{275-272} \text{ if } 272 < T < 275 \\ 0 \text{ if } T \geq 275 \end{cases} \tag{A3}$$

Author contributions. Experimental design, setup and simulations: ÅB and JB, analysis, visualization and draft writing: ÅB, review and editing: JB and MM.

445 *Competing interests.* The authors declare that they have no conflict of interest.

Acknowledgements. The work in this paper was conducted as part of The Copernicus Climate Change Service Evolution (CERISE) project (grant agreement No101082139), funded by the European Union. Views and opinions expressed are however those of the author(s) only and do not necessarily reflect those of the European Union or the Commission. Neither the European Union nor the granting authority can be held responsible for them.

450 References

Aas, K. S., Gisnås, K., Westermann, S., and Berntsen, T. K.: A Tiling Approach to Represent Subgrid Snow Variability in Coupled Land Surface–Atmosphere Models, Journal of Hydrometeorology, https://doi.org/10.1175/JHM-D-16-0026.1, section: Journal of Hydrometeorology, 2017.

Alonso-González, E., Gascoin, S., Arioli, S., and Picard, G.: Exploring the potential of thermal infrared remote sensing to improve a snowpack model through an observing system simulation experiment, The Cryosphere, 17, 3329–3342, https://doi.org/10.5194/tc-17-3329-2023, publisher: Copernicus GmbH, 2023.

Arduini, G., Balsamo, G., Dutra, E., Day, J. J., Sandu, I., Boussetta, S., and Haiden, T.: Impact of a Multi-Layer Snow Scheme on Near-Surface Weather Forecasts, Journal of Advances in Modeling Earth Systems, 11, 4687–4710, https://doi.org/10.1029/2019MS001725, _eprint: https://onlinelibrary.wiley.com/doi/pdf/10.1029/2019MS001725, 2019.

Bengtsson, L., Andrae, U., Aspelien, T., Batrak, Y., Calvo, J., de Rooy, W., Gleeson, E., Hansen-Sass, B., Homleid, M., Hortal, M., Ivarsson, K.-I., Lenderink, G., Niemelä, S., Nielsen, K. P., Onvlee, J., Rontu, L., Samuelsson, P., Muñoz, D. S., Subias, A., Tijm, S., Toll, V., Yang, X., and Køltzow, M. Ø.: The HARMONIE–AROME Model Configuration in the ALADIN–HIRLAM NWP System, Monthly Weather Review, 145, 1919–1935, https://doi.org/10.1175/MWR-D-16-0417.1, publisher: American Meteorological Society, 2017.

Blyverket, J., Hamer, P. D., Bertino, L., Albergel, C., Fairbairn, D., and Lahoz, W. A.: An Evaluation of the EnKF vs. EnOI and the Assimilation of SMAP, SMOS and ESA CCI Soil Moisture Data over the Contiguous US, Remote Sensing, 11, 478, https://doi.org/10.3390/rs11050478, number: 5 Publisher: Multidisciplinary Digital Publishing Institute, 2019.

Boone, A., Samuelsson, P., Gollvik, S., Napoly, A., Jarlan, L., Brun, E., and Decharme, B.: The interactions between soil–biosphere–atmosphere land surface model with a multi-energy balance (ISBA-MEB) option in SURFEXv8 – Part 1: Model description, Geoscientific Model Development, 10, 843–872, https://doi.org/10.5194/gmd-10-843-2017, publisher: Copernicus GmbH, 2017.

Box, J. E., Nielsen, K. P., Yang, X., Niwano, M., Wehrlé, A., van As, D., Fettweis, X., Køltzow, M. A. Ø., Palmason, B., Fausto, R. S., van den Broeke, M. R., Huai, B., Ahlstrøm, A. P., Langley, K., Dachauer, A., and Noël, B.: Greenland ice sheet rainfall climatology, extremes and atmospheric river rapids, Meteorological Applications, 30, e2134, https://doi.org/10.1002/met.2134, _eprint: https://onlinelibrary.wiley.com/doi/pdf/10.1002/met.2134, 2023.

Brangers, I., Lievens, H., Getirana, A., and De Lannoy, G. J. M.: Sentinel-1 Snow Depth Assimilation to Improve River Discharge Estimates in the Western European Alps, Water Resources Research, 60, e2023WR035 019, https://doi.org/10.1029/2023WR035019, _eprint: https://onlinelibrary.wiley.com/doi/pdf/10.1029/2023WR035019, 2024.

Brasnett, B.: A Global Analysis of Snow Depth for Numerical Weather Prediction, Journal of Applied Meteorology and Climatology, https://journals.ametsoc.org/view/journals/apme/38/6/1520-0450_1999_038_0726_agaosd_2.0.co_2.xml, section: Journal of Applied Meteorology and Climatology, 1999.

Calvet, J.-C., Noilhan, J., Roujean, J.-L., Bessemoulin, P., Cabelguenne, M., Olioso, A., and Wigneron, J.-P.: An interactive vegetation SVAT model tested against data from six contrasting sites, Agricultural and Forest Meteorology, 92, 73–95, https://doi.org/10.1016/S0168-1923(98)00091-4, 1998.

Cao, B., Gruber, S., Zheng, D., and Li, X.: The ERA5-Land soil temperature bias in permafrost regions, The Cryosphere, 14, 2581–2595, https://doi.org/10.5194/tc-14-2581-2020, publisher: Copernicus GmbH, 2020.

485 Casson, D. R., Werner, M., Weerts, A., and Solomatine, D.: Global re-analysis datasets to improve hydrological assessment and snow water equivalent estimation in a sub-Arctic watershed, Hydrology and Earth System Sciences, 22, 4685–4697, https://doi.org/10.5194/hess-22-4685-2018, publisher: Copernicus GmbH, 2018.

Charrois, L., Cosme, E., Dumont, M., Lafaysse, M., Morin, S., Libois, Q., and Picard, G.: On the assimilation of optical reflectances and snow depth observations into a detailed snowpack model, The Cryosphere, 10, 1021–1038, https://doi.org/10.5194/tc-10-1021-2016, publisher:
490 Copernicus GmbH, 2016.

Clelland, A. A., Marshall, G. J., and Baxter, R.: Evaluating the performance of key ERA-Interim, ERA5 and ERA5-Land climate variables across Siberia, International Journal of Climatology, 44, 2318–2342, https://doi.org/10.1002/joc.8456, _eprint: https://onlinelibrary.wiley.com/doi/pdf/10.1002/joc.8456, 2024.

Cluzet, B., Lafaysse, M., Cosme, E., Albergel, C., Meunier, L.-F., and Dumont, M.: CrocO_v1.0: a particle filter to assimilate snowpack
495 observations in a spatialised framework, Geoscientific Model Development, 14, 1595–1614, https://doi.org/10.5194/gmd-14-1595-2021, 2021.

Cluzet, B., Lafaysse, M., Deschamps-Berger, C., Vernay, M., and Dumont, M.: Propagating information from snow observations with CrocO ensemble data assimilation system: a 10-years case study over a snow depth observation network, The Cryosphere, 16, 1281–1298, https://doi.org/10.5194/tc-16-1281-2022, publisher: Copernicus GmbH, 2022.

500 Croce, P., Formichi, P., Landi, F., Mercogliano, P., Bucchignani, E., Dosio, A., and Dimova, S.: The snow load in Europe and the climate change, Climate Risk Management, 20, 138–154, https://doi.org/10.1016/j.crm.2018.03.001, 2018.

De Lannoy, G. J. M., Reichle, R. H., Arsenault, K. R., Houser, P. R., Kumar, S., Verhoest, N. E. C., and Pauwels, V. R. N.: Multiscale assimilation of Advanced Microwave Scanning Radiometer–EOS snow water equivalent and Moderate Resolution Imaging Spectroradiometer snow cover fraction observations in northern Colorado, Water Resources Research, 48, https://doi.org/10.1029/2011WR010588, _eprint:
505 https://onlinelibrary.wiley.com/doi/pdf/10.1029/2011WR010588, 2012.

de Rosnay, P., Balsamo, G., Albergel, C., Muñoz-Sabater, J., and Isaksen, L.: Initialisation of Land Surface Variables for Numerical Weather Prediction, Surveys in Geophysics, 35, 607–621, https://doi.org/10.1007/s10712-012-9207-x, 2014.

Decharme, B., Boone, A., Delire, C., and Noilhan, J.: Local evaluation of the Interaction between Soil Biosphere Atmosphere soil multilayer diffusion scheme using four pedotransfer functions, Journal of Geophysical Research: Atmospheres, 116,
510 https://doi.org/https://doi.org/10.1029/2011JD016002, _eprint: https://agupubs.onlinelibrary.wiley.com/doi/pdf/10.1029/2011JD016002, 2011.

Decharme, B., Brun, E., Boone, A., Delire, C., Le Moigne, P., and Morin, S.: Impacts of snow and organic soils parameterization on northern Eurasian soil temperature profiles simulated by the ISBA land surface model, The Cryosphere, 10, 853–877, https://doi.org/https://doi.org/10.5194/tc-10-853-2016, publisher: Copernicus GmbH, 2016.

515 Diefenbach, T., Craig, G., Keil, C., Scheck, L., and Weissmann, M.: Partial analysis increments as diagnostic for LETKF data assimilation systems, Quarterly Journal of the Royal Meteorological Society, 149, 740–756, https://doi.org/10.1002/qj.4419, _eprint: https://onlinelibrary.wiley.com/doi/pdf/10.1002/qj.4419, 2023.

Douville, H., Royer, J. F., and Mahfouf, J. F.: A new snow parameterization for the Météo-France climate model, Climate Dynamics, 12, 21–35, https://doi.org/10.1007/BF00208760, 1995.

520 Draper, C. S.: Accounting for Land Model Uncertainty in Numerical Weather Prediction Ensemble Systems: Toward Ensemble-Based Coupled Land–Atmosphere Data Assimilation, Journal of Hydrometeorology, 22, 2089–2104, https://doi.org/10.1175/JHM-D-21-0016.1, publisher: American Meteorological Society Section: Journal of Hydrometeorology, 2021.

Durand, M. and Margulis, S. A.: Correcting first-order errors in snow water equivalent estimates using a multifrequency, multiscale radio-metric data assimilation scheme, Journal of Geophysical Research: Atmospheres, 112, https://doi.org/10.1029/2006JD008067, _eprint:
525   https://onlinelibrary.wiley.com/doi/pdf/10.1029/2006JD008067, 2007.

Egli, L., Jonas, T., and Meister, R.: Comparison of different automatic methods for estimating snow water equivalent, Cold Regions Science and Technology, 57, 107–115, https://doi.org/10.1016/j.coldregions.2009.02.008, 2009.

Evensen, G.: The Ensemble Kalman Filter: theoretical formulation and practical implementation, Ocean Dynamics, 53, 343–367, https://doi.org/10.1007/s10236-003-0036-9, 2003.

530   Fisher, R. A. and Koven, C. D.: Perspectives on the Future of Land Surface Models and the Challenges of Representing Complex Terrestrial Systems, Journal of Advances in Modeling Earth Systems, 12, e2018MS001 453, https://doi.org/10.1029/2018MS001453, _eprint: https://onlinelibrary.wiley.com/doi/pdf/10.1029/2018MS001453, 2020.

Gaspari, G. and Cohn, S. E.: Construction of correlation functions in two and three dimensions, Quarterly Journal of the Royal Meteorological Society, 125, 723–757, https://doi.org/10.1002/qj.49712555417, _eprint:
535   https://onlinelibrary.wiley.com/doi/pdf/10.1002/qj.49712555417, 1999.

Gastaldo, T., Poli, V., Marsigli, C., Alberoni, P. P., and Paccagnella, T.: Data assimilation of radar reflectivity volumes in a LETKF scheme, Nonlinear Processes in Geophysics, 25, 747–764, https://doi.org/10.5194/npg-25-747-2018, publisher: Copernicus GmbH, 2018.

Gelaro, R., McCarty, W., Suárez, M. J., Todling, R., Molod, A., Takacs, L., Randles, C. A., Darmenov, A., Bosilovich, M. G., Reichle, R., Wargan, K., Coy, L., Cullather, R., Draper, C., Akella, S., Buchard, V., Conaty, A., Silva, A. M. d., Gu, W., Kim, G.-K., Koster,
540   R., Lucchesi, R., Merkova, D., Nielsen, J. E., Partyka, G., Pawson, S., Putman, W., Rienecker, M., Schubert, S. D., Sienkiewicz, M., and Zhao, B.: The Modern-Era Retrospective Analysis for Research and Applications, Version 2 (MERRA-2), Journal of Climate, https://doi.org/10.1175/JCLI-D-16-0758.1, section: Journal of Climate, 2017.

Gichamo, T. Z. and Draper, C. S.: An Optimal Interpolation–Based Snow Data Assimilation for NOAA's Unified Forecast System (UFS), Weather and Forecasting, https://doi.org/10.1175/WAF-D-22-0061.1, section: Weather and Forecasting, 2022.

545   Gisnås, K., Westermann, S., Schuler, T. V., Melvold, K., and Etzelmüller, B.: Small-scale variation of snow in a regional permafrost model, The Cryosphere, 10, 1201–1215, https://doi.org/10.5194/tc-10-1201-2016, publisher: Copernicus GmbH, 2016.

Gong, G., Entekhabi, D., Cohen, J., and Robinson, D.: Sensitivity of atmospheric response to modeled snow anomaly characteristics, Journal of Geophysical Research: Atmospheres, 109, https://doi.org/10.1029/2003JD004160, _eprint: https://onlinelibrary.wiley.com/doi/pdf/10.1029/2003JD004160, 2004.

550   Hedrick, A. R., Marks, D., Havens, S., Robertson, M., Johnson, M., Sandusky, M., Marshall, H.-P., Kormos, P. R., Bormann, K. J., and Painter, T. H.: Direct Insertion of NASA Airborne Snow Observatory-Derived Snow Depth Time Series Into the iSnobal Energy Balance Snow Model, Water Resources Research, 54, 8045–8063, https://doi.org/10.1029/2018WR023190, _eprint: https://onlinelibrary.wiley.com/doi/pdf/10.1029/2018WR023190, 2018.

Helmert, J., Şensoy Şorman, A., Alvarado Montero, R., De Michele, C., De Rosnay, P., Dumont, M., Finger, D. C., Lange, M., Pi-
555   card, G., Potopová, V., Pullen, S., Vikhamar-Schuler, D., and Arslan, A. N.: Review of Snow Data Assimilation Methods for Hydrological, Land Surface, Meteorological and Climate Models: Results from a COST HarmoSnow Survey, Geosciences, 8, 489, https://doi.org/10.3390/geosciences8120489, number: 12 Publisher: Multidisciplinary Digital Publishing Institute, 2018.

Hengl, T., Jesus, J. M. d., Heuvelink, G. B. M., Gonzalez, M. R., Kilibarda, M., Blagotić, A., Shangguan, W., Wright, M. N., Geng, X., Bauer-Marschallinger, B., Guevara, M. A., Vargas, R., MacMillan, R. A., Batjes, N. H., Leenaars, J. G. B., Ribeiro, E., Wheeler, I.,

560   Mantel, S., and Kempen, B.: SoilGrids250m: Global gridded soil information based on machine learning, PLOS ONE, 12, e0169 748, https://doi.org/10.1371/journal.pone.0169748, publisher: Public Library of Science, 2017.

Herbert, C., de Rosnay, P., Weston, P., and Fairbairn, D.: Towards unified land data assimilation at ECMWF: Soil and snow temperature analysis in the SEKF, Quarterly Journal of the Royal Meteorological Society, 150, 4133–4155, https://doi.org/10.1002/qj.4808, _eprint: https://onlinelibrary.wiley.com/doi/pdf/10.1002/qj.4808, 2024.

565   Hersbach, H., Bell, B., Berrisford, P., Hirahara, S., Horányi, A., Muñoz-Sabater, J., Nicolas, J., Peubey, C., Radu, R., Schepers, D., Simmons, A., Soci, C., Abdalla, S., Abellan, X., Balsamo, G., Bechtold, P., Biavati, G., Bidlot, J., Bonavita, M., De Chiara, G., Dahlgren, P., Dee, D., Diamantakis, M., Dragani, R., Flemming, J., Forbes, R., Fuentes, M., Geer, A., Haimberger, L., Healy, S., Hogan, R. J., Hólm, E., Janisková, M., Keeley, S., Laloyaux, P., Lopez, P., Lupu, C., Radnoti, G., de Rosnay, P., Rozum, I., Vamborg, F., Villaume, S., and Thépaut, J.-N.: The ERA5 global reanalysis, Quarterly Journal of the Royal Meteorological Society, 146, 1999–2049,
570   https://doi.org/10.1002/qj.3803, _eprint: https://onlinelibrary.wiley.com/doi/pdf/10.1002/qj.3803, 2020.

Homleid, M. and Killi, M. A.: HARMONIE snow analysis experiments with additional observations, Tech. Rep. 06/2013, Norwegian Meteorological Institute, https://www.met.no/publikasjoner/met-report/met-report-2013, 2014.

Hunt, B. R., Kostelich, E. J., and Szunyogh, I.: Efficient data assimilation for spatiotemporal chaos: A local ensemble transform Kalman filter, Physica D: Nonlinear Phenomena, 230, 112–126, https://doi.org/10.1016/j.physd.2006.11.008, 2007.

575   Katzfuss, M., Stroud, J. R., and Wikle, C. K.: Understanding the Ensemble Kalman Filter, The American Statistician, 70, 350–357, https://doi.org/10.1080/00031305.2016.1141709, 2016.

Koohkan, M. R. and Bocquet, M.: Accounting for representativeness errors in the inversion of atmospheric constituent emissions: application to the retrieval of regional carbon monoxide fluxes, Tellus B: Chemical and Physical Meteorology, 64, https://doi.org/10.3402/tellusb.v64i0.19047, 2012.

580   Kouki, K., Luojus, K., and Riihelä, A.: Evaluation of snow cover properties in ERA5 and ERA5-Land with several satellite-based datasets in the Northern Hemisphere in spring 1982–2018, The Cryosphere, 17, 5007–5026, https://doi.org/10.5194/tc-17-5007-2023, publisher: Copernicus GmbH, 2023.

Kumar, S. V., Peters-Lidard, C. D., Mocko, D., Reichle, R., Liu, Y., Arsenault, K. R., Xia, Y., Ek, M., Riggs, G., Livneh, B., and Cosh, M.: Assimilation of Remotely Sensed Soil Moisture and Snow Depth Retrievals for Drought Estimation, Journal of Hydrometeorology,
585   https://doi.org/10.1175/JHM-D-13-0132.1, section: Journal of Hydrometeorology, 2014.

Kumar, S. V., Dong, J., Peters-Lidard, C. D., Mocko, D., and Gómez, B.: Role of forcing uncertainty and background model error characterization in snow data assimilation, Hydrology and Earth System Sciences, 21, 2637–2647, https://doi.org/10.5194/hess-21-2637-2017, publisher: Copernicus GmbH, 2017.

Kwon, Y., Forman, B. A., Ahmad, J. A., Kumar, S. V., and Yoon, Y.: Exploring the Utility of Machine Learning-Based Passive
590   Microwave Brightness Temperature Data Assimilation over Terrestrial Snow in High Mountain Asia, Remote Sensing, 11, 2265, https://doi.org/10.3390/rs11192265, number: 19 Publisher: Multidisciplinary Digital Publishing Institute, 2019.

Køltzow, M., Schyberg, H., Støylen, E., and Yang, X.: Value of the Copernicus Arctic Regional Reanalysis (CARRA) in representing near-surface temperature and wind speed in the north-east European Arctic, Polar Research, 41, https://doi.org/10.33265/polar.v41.8002, 2022.

Lannoy, G. J. M. D., Reichle, R. H., Houser, P. R., Arsenault, K. R., Verhoest, N. E. C., and Pauwels, V. R. N.: Satellite-Scale
595   Snow Water Equivalent Assimilation into a High-Resolution Land Surface Model, Journal of Hydrometeorology, 11, 352–369, https://doi.org/10.1175/2009JHM1192.1, publisher: American Meteorological Society Section: Journal of Hydrometeorology, 2010.

Le Coz, C., Heemink, A., Verlaan, M., ten Veldhuis, M.-c., and van de Giesen, N.: Correcting Position Error in Precipitation Data Using Image Morphing, Remote Sensing, 11, 2557, https://doi.org/10.3390/rs11212557, number: 21 Publisher: Multidisciplinary Digital Publishing Institute, 2019.

600 Lee, J., Lee, M.-I., Tak, S., Seo, E., and Lee, Y.-K.: Assimilation of snow water equivalent from AMSR2 and IMS satellite data utilizing the local ensemble transform Kalman filter, Geoscientific Model Development, 17, 8799–8816, https://doi.org/10.5194/gmd-17-8799-2024, publisher: Copernicus GmbH, 2024.

Leutbecher, M.: Ensemble size: How suboptimal is less than infinity?, Quarterly Journal of the Royal Meteorological Society, 145, 107–128, https://doi.org/10.1002/qj.3387, _eprint: https://onlinelibrary.wiley.com/doi/pdf/10.1002/qj.3387, 2019.

605 Li, D., Lettenmaier, D. P., Margulis, S. A., and Andreadis, K.: The Value of Accurate High-Resolution and Spatially Continuous Snow Information to Streamflow Forecasts, Journal of Hydrometeorology, https://doi.org/10.1175/JHM-D-18-0210.1, section: Journal of Hydrometeorology, 2019.

Li, W., Chen, J., Li, L., Orsolini, Y. J., Xiang, Y., Senan, R., and de Rosnay, P.: Impacts of snow assimilation on seasonal snow and meteorological forecasts for the Tibetan Plateau, The Cryosphere, 16, 4985–5000, https://doi.org/10.5194/tc-16-4985-2022, publisher: Copernicus

610 GmbH, 2022.

Liston, G. E. and Hiemstra, C. A.: A Simple Data Assimilation System for Complex Snow Distributions (SnowAssim), Journal of Hydrometeorology, https://doi.org/10.1175/2008JHM871.1, section: Journal of Hydrometeorology, 2008.

Liu, Q., Reichle, R. H., Bindlish, R., Cosh, M. H., Crow, W. T., Jeu, R. d., Lannoy, G. J. M. D., Huffman, G. J., and Jackson, T. J.: The Contributions of Precipitation and Soil Moisture Observations to the Skill of Soil Moisture Estimates in a Land Data Assimilation System,

615 Journal of Hydrometeorology, https://doi.org/10.1175/JHM-D-10-05000.1, section: Journal of Hydrometeorology, 2011.

Maggioni, V., Reichle, R. H., and Anagnostou, E. N.: The Impact of Rainfall Error Characterization on the Estimation of Soil Moisture Fields in a Land Data Assimilation System, Journal of Hydrometeorology, https://doi.org/10.1175/JHM-D-11-0115.1, section: Journal of Hydrometeorology, 2012.

Magnusson, J., Winstral, A., Stordal, A. S., Essery, R., and Jonas, T.: Improving physically based snow simulations by assimilat-

620 ing snow depths using the particle filter, Water Resources Research, 53, 1125–1143, https://doi.org/10.1002/2016WR019092, _eprint: https://onlinelibrary.wiley.com/doi/pdf/10.1002/2016WR019092, 2017.

Magnusson, J., Nævdal, G., Matt, F., Burkhart, J. F., and Winstral, A.: Improving hydropower inflow forecasts by assimilating snow data, Hydrology Research, 51, 226–237, https://doi.org/10.2166/nh.2020.025, 2020.

Masson, V., Moigne, P. L., Martin, E., Faroux, S., Alias, A., Alkama, R., Belamari, S., Barbu, A., Boone, A., Bouyssel, F., Brousseau, P.,

625 Brun, E., Calvet, J.-C., Carrer, D., Decharme, B., Delire, C., Donier, S., Essaouini, K., Gibelin, A.-L., Giordani, H., Habets, F., Jidane, M., Kerdraon, G., Kourzeneva, E., Lafaysse, M., Lafont, S., Lebeaupin Brossier, C., Lemonsu, A., Mahfouf, J.-F., Marguinaud, P., Mokhtari, M., Morin, S., Pigeon, G., Salgado, R., Seity, Y., Taillefer, F., Tanguy, G., Tulet, P., Vincendon, B., Vionnet, V., and Voldoire, A.: The SURFEXv7.2 land and ocean surface platform for coupled or offline simulation of earth surface variables and fluxes, Geoscientific Model Development, 6, 929–960, https://doi.org/https://doi.org/10.5194/gmd-6-929-2013, publisher: Copernicus GmbH, 2013.

630 Micheletty, P., Perrot, D., Day, G., and Rittger, K.: Assimilation of Ground and Satellite Snow Observations in a Distributed Hydrologic Model for Water Supply Forecasting, JAWRA Journal of the American Water Resources Association, 58, 1030–1048, https://doi.org/10.1111/1752-1688.12975, _eprint: https://onlinelibrary.wiley.com/doi/pdf/10.1111/1752-1688.12975, 2022.

Monteiro, D., Caillaud, C., Lafaysse, M., Napoly, A., Fructus, M., Alias, A., and Morin, S.: Improvements in the land surface configuration to better simulate seasonal snow cover in the European Alps with the CNRM-AROME (cycle 46) convection-permitting regional

635   climate model, Geoscientific Model Development, 17, 7645–7677, https://doi.org/10.5194/gmd-17-7645-2024, publisher: Copernicus GmbH, 2024.

Muñoz-Sabater, J., Dutra, E., Agustí-Panareda, A., Albergel, C., Arduini, G., Balsamo, G., Boussetta, S., Choulga, M., Harrigan, S., Hersbach, H., Martens, B., Miralles, D. G., Piles, M., Rodríguez-Fernández, N. J., Zsoter, E., Buontempo, C., and Thépaut, J.-N.: ERA5-Land: a state-of-the-art global reanalysis dataset for land applications, Earth System Science Data, 13, 4349–4383, https://doi.org/10.5194/essd-
640   13-4349-2021, publisher: Copernicus GmbH, 2021.

Napoly, A., Boone, A., Samuelsson, P., Gollvik, S., Martin, E., Seferian, R., Carrer, D., Decharme, B., and Jarlan, L.: The interactions between soil–biosphere–atmosphere (ISBA) land surface model multi-energy balance (MEB) option in SURFEXv8 – Part 2: Introduction of a litter formulation and model evaluation for local-scale forest sites, Geoscientific Model Development, 10, 1621–1644, https://doi.org/10.5194/gmd-10-1621-2017, 2017.

645   Nerger, L.: Data assimilation for nonlinear systems with a hybrid nonlinear Kalman ensemble transform filter, Quarterly Journal of the Royal Meteorological Society, 148, 620–640, https://doi.org/10.1002/qj.4221, _eprint: https://onlinelibrary.wiley.com/doi/pdf/10.1002/qj.4221, 2022.

Noilhan, J. and Mahfouf, J. F.: The ISBA land surface parameterisation scheme, Global and Planetary Change, 13, 145–159, https://doi.org/10.1016/0921-8181(95)00043-7, 1996.

650   Oberrauch, M., Cluzet, B., Magnusson, J., and Jonas, T.: Improving Fully Distributed Snowpack Simulations by Mapping Perturbations of Meteorological Forcings Inferred From Particle Filter Assimilation of Snow Monitoring Data, Water Resources Research, 60, e2023WR036 994, https://doi.org/10.1029/2023WR036994, _eprint: https://onlinelibrary.wiley.com/doi/pdf/10.1029/2023WR036994, 2024.

Picard, G., Sandells, M., and Löwe, H.: SMRT: an active–passive microwave radiative transfer model for snow with multiple microstruc-
655   ture and scattering formulations (v1.0), Geoscientific Model Development, 11, 2763–2788, https://doi.org/10.5194/gmd-11-2763-2018, publisher: Copernicus GmbH, 2018.

Reichle, R. H. and Koster, R. D.: Assessing the Impact of Horizontal Error Correlations in Background Fields on Soil Moisture Estimation, Journal of Hydrometeorology, https://journals.ametsoc.org/view/journals/hydr/4/6/1525-7541_2003_004_1229_atiohe_2_0_co_2.xml, section: Journal of Hydrometeorology, 2003.

660   Ridal, M., Bazile, E., Le Moigne, P., Randriamampianina, R., Schimanke, S., Andrae, U., Berggren, L., Brousseau, P., Dahlgren, P., Edvinsson, L., El-Said, A., Glinton, M., Hagelin, S., Hopsch, S., Isaksson, L., Medeiros, P., Olsson, E., Unden, P., and Wang, Z. Q.: CERRA, the Copernicus European Regional Reanalysis system, Quarterly Journal of the Royal Meteorological Society, 150, 3385–3411, https://doi.org/10.1002/qj.4764, _eprint: https://onlinelibrary.wiley.com/doi/pdf/10.1002/qj.4764, 2024.

Sakov, P. and Bertino, L.: Relation between two common localisation methods for the EnKF, Computational Geosciences, 15, 225–237,
665   https://doi.org/10.1007/s10596-010-9202-6, 2011.

Schyberg H., Yang X., Køltzow M.A.Ø., Amstrup B., Bakketun Å., Bazile E., Bojarova J., Box J. E., Dahlgren P., Hagelin S., Homleid M., Horányi A., Høyer J., Johansson Å., Killie M.A., Körnich H., Le Moigne P., Lindskog M., Manninen T., Nielsen Englyst P., Nielsen K.P., Olsson E., Palmason B., Peralta Aros C., Randriamampianina R., Samuelsson P., Stappers R., Støylen E., Thorsteinsson S., Valkonen T., Wang Z.Q, and Copernicus Climate Change Service: Arctic regional reanalysis on single levels from 1991 to present,
670   https://doi.org/10.24381/CDS.713858F6, 2021.

Seo, E., Lee, M.-I., and Reichle, R. H.: Assimilation of SMAP and ASCAT soil moisture retrievals into the JULES land surface model using the Local Ensemble Transform Kalman Filter, Remote Sensing of Environment, 253, 112 222, https://doi.org/10.1016/j.rse.2020.112222, 2021.

Shin, S., Kang, J.-S., and Jo, Y.: The Local Ensemble Transform Kalman Filter (LETKF) with a Global NWP Model on the Cubed Sphere, Pure and Applied Geophysics, 173, 2555–2570, https://doi.org/10.1007/s00024-016-1269-0, 2016.

Slater, A. G. and Clark, M. P.: Snow Data Assimilation via an Ensemble Kalman Filter, Journal of Hydrometeorology, 7, 478–493, https://doi.org/10.1175/JHM505.1, publisher: American Meteorological Society Section: Journal of Hydrometeorology, 2006.

Smyth, E. J., Raleigh, M. S., and Small, E. E.: Improving SWE Estimation With Data Assimilation: The Influence of Snow Depth Observation Timing and Uncertainty, Water Resources Research, 56, e2019WR026 853, https://doi.org/10.1029/2019WR026853, _eprint: https://onlinelibrary.wiley.com/doi/pdf/10.1029/2019WR026853, 2020.

Sturm, M., Goldstein, M. A., and Parr, C.: Water and life from snow: A trillion dollar science question, Water Resources Research, 53, 3534–3544, https://doi.org/10.1002/2017WR020840, _eprint: https://onlinelibrary.wiley.com/doi/pdf/10.1002/2017WR020840, 2017.

Tippett, M. K., Anderson, J. L., Bishop, C. H., Hamill, T. M., and Whitaker, J. S.: Ensemble Square Root Filters, Monthly Weather Review, 131, 1485–1490, https://doi.org/10.1175/1520-0493(2003)131<1485:ESRF>2.0.CO;2, publisher: American Meteorological Society Section: Monthly Weather Review, 2003.

Tollan, A.: Experiences with snow pillows in norway, International Association of Scientific Hydrology. Bulletin, 15, 113–120, https://doi.org/10.1080/02626667009493958, publisher: Taylor & Francis, 1970.

Viviroli, D., Dürr, H. H., Messerli, B., Meybeck, M., and Weingartner, R.: Mountains of the world, water towers for humanity: Typology, mapping, and global significance, Water Resources Research, 43, https://doi.org/10.1029/2006WR005653, _eprint: https://onlinelibrary.wiley.com/doi/pdf/10.1029/2006WR005653, 2007.

Yin, J., Zhan, X., Zheng, Y., Hain, C. R., Liu, J., and Fang, L.: Optimal ensemble size of ensemble Kalman filter in sequential soil moisture data assimilation, Geophysical Research Letters, 42, 6710–6715, https://doi.org/10.1002/2015GL063366, _eprint: https://onlinelibrary.wiley.com/doi/pdf/10.1002/2015GL063366, 2015.

Zsoter, E., Arduini, G., Prudhomme, C., Stephens, E., and Cloke, H.: Hydrological Impact of the New ECMWF Multi-Layer Snow Scheme, Atmosphere, 13, 727, https://doi.org/10.3390/atmos13050727, number: 5 Publisher: Multidisciplinary Digital Publishing Institute, 2022.